

Geophysical Research Letters[®]

RESEARCH LETTER

10.1029/2023GL107140

The Climatology of Mars Thermospheric Polar Warming at Aphelion



Key Points:

- Thermospheric polar warming is observed at Mars during aphelion at dawn
- A significant enhancement of thermospheric polar warming coincides with a dust storm in the summer hemisphere (MY 34)
- Thermospheric polar warming is evident at dawn local times in two independent solar occultation data sets from two spacecraft, Mars Atmosphere and Volatile Evolution and Trace Gas Orbiter

Correspondence to:

E. M. B. Thiemann,
thiemann@lasp.colorado.edu

Citation:

Thiemann, E. M. B., Trompet, L., Bougher, S. W., Yiğit, E., Gasperini, F., Montabone, L., et al. (2024). The climatology of Mars thermospheric polar warming at aphelion. *Geophysical Research Letters*, 51, e2023GL107140. <https://doi.org/10.1029/2023GL107140>








Received 6 NOV 2023
Accepted 21 FEB 2024

Author Contributions:

Conceptualization: Edward M. B. Thiemann, Loïc Trompet, Francisco Gonzalez-Galindo
Data curation: Luca Montabone, Francis G. Eparvier, Anne-Carine Vandaele
Formal analysis: Edward M. B. Thiemann, Loïc Trompet, Stephen W. Bougher, Erdal Yiğit, Federico Gasperini, Luca Montabone
Funding acquisition: Edward M. B. Thiemann
Investigation: Edward M. B. Thiemann, Loïc Trompet, Stephen W. Bougher, Erdal Yiğit, Federico Gasperini, Luca Montabone
Methodology: Edward M. B. Thiemann
Project administration: Edward M. B. Thiemann
Resources: Edward M. B. Thiemann, Francis G. Eparvier, Anne-Carine Vandaele

© 2024. The Authors.

This is an open access article under the terms of the [Creative Commons Attribution License](https://creativecommons.org/licenses/by/4.0/), which permits use, distribution and reproduction in any medium, provided the original work is properly cited.

Edward M. B. Thiemann¹ , Loïc Trompet² , Stephen W. Bougher³ , Erdal Yiğit⁴ , Federico Gasperini⁵ , Luca Montabone⁶ , Francisco Gonzalez-Galindo⁷ , Francis G. Eparvier¹, and Anne-Carine Vandaele²

¹Laboratory for Atmospheric and Space Physics, University of Colorado Boulder, Boulder, CO, USA, ²Royal Belgian Institute for Space Aeronomy, Uccle, Belgium, ³Department of Climate and Space Sciences and Engineering, University of Michigan, Ann Arbor, MI, USA, ⁴Department of Physics and Astronomy, Space Weather Lab, George Mason University, Fairfax, VA, USA, ⁵Orion Space Solutions, Louisville, CO, USA, ⁶Panureka, Le Bourget-du-Lac, France, ⁷Instituto de Astrofísica de Andalucía-CSIC, Granada, Spain

Abstract Thermospheric polar warming (TPW) is observed conclusively for the first time at Mars during the aphelion/Northern Summer season using solar occultation (SO) measurements made by the Extreme Ultraviolet Monitor (EUVM) onboard the Mars Atmosphere and Volatile Evolution (MAVEN) orbiter. Aphelion data from Mars Year (MY) 33–36 are analyzed revealing TPW to be present at dawn but not dusk. This is consistent with an earlier analysis of accelerometer data from the Mars Global Surveyor that showed aphelion TPW is also not evident at 15 hr local time. Separating the data into individual MYs reveals TPW is observed during each year except MY 35. TPW is markedly intensified during MY 34, which is attributed to enhanced circulation caused by a northern-hemisphere dust storm coinciding with the observations. Simulations from the Mars Climate Database predict the large TPW enhancement in MY 34 relative to MY 33 observed by EUVM SO, but predicts approximately 20K less overall TPW for both years than that observed by EUVM SO.

Plain Language Summary Warming in the winter upper atmosphere has been observed for the first time in the Southern hemisphere at Mars during aphelion, when Mars is furthest from the Sun, using the Extreme Ultraviolet Monitor onboard the Mars Atmosphere and Volatile Evolution orbiter. These observations show the warming trend is typically found at dawn but is not observed at dusk. This warming is believed to be caused by large-scale atmospheric circulation that transports air from the warmer summer hemisphere toward the winter pole. These observations show that the winter upper atmospheric warming is most pronounced when a dust storm is active in the summer hemisphere, which can be explained by the dust storm strengthening the circulation pattern responsible for the warming. These measurements are compared to simulations from an atmospheric model (called the Mars Climate Database) that show reasonably good agreement.

1. Introduction

Thermospheric Polar Warming (TPW) is an example of a dynamical heating phenomenon occurring at Mars that can significantly influence its thermospheric temperature. TPWs are a manifestation of global-scale meridional transport, similar to the phenomenon of middle atmospheric polar warming (e.g., Medvedev & Hartogh, 2007). Aside from the higher altitude range, TPW is distinguished from polar warming in the middle atmosphere by its sensitivity to tidal features unique to the thermosphere. TPW occurs in the winter hemisphere near the solstices. Qualitatively, it is caused by a global-scale meridional circulation cell with the ascending leg in the summer hemisphere dayside and the descending leg on the nightside of the winter hemisphere. This descending leg adiabatically heats the high-latitude winter hemisphere. TPW near perihelion was first reported by Bougher et al. (2006), who, using temperatures derived from accelerometer measurements made by the Mars Odyssey orbiter, identified a warming trend at 120 km altitude with increasing latitude in the northern winter hemisphere on the nightside. Bougher et al. (2006) found no evidence of TPW near aphelion from accelerometer measurements made by the Mars Global Surveyor (MGS) orbiter, but the majority of the data coinciding with aphelion were measured on the dayside, where TPW may be less pronounced based on subsequent global circulation model (GCM) simulations by Gonzalez-Galindo et al. (2009) that showed TPW heating to be concentrated on the nightside.

Software: Edward M. B. Thiemann
Supervision: Anne-Carine Vandaele
Validation: Edward M. B. Thiemann
Visualization: Loïc Trompet,
 Luca Montabone
Writing – original draft: Edward
 M. B. Thiemann
Writing – review & editing: Edward
 M. B. Thiemann, Loïc Trompet, Stephen
 W. Bougher, Erdal Yiğit,
 Federico Gasperini, Luca Montabone

GCM simulations have shown that TPW depends on dust in the summer hemisphere, plus vertically propagating tides and gravity waves. Bell et al. (2007) showed that TPW increases with increasing dust in the lower atmosphere of the summer hemisphere and that the main driver of warming is from a meridional circulation cell originating below 70 km in the summer hemisphere. Simulations show that TPW is present at both solstices, but the TPW amplitude is less significant and shifted $\sim 15^\circ$ equatorward at the solstice near aphelion (solar longitude (L_s) = 90°) than that near perihelion (L_s = 270°), peaking near 70°S at aphelion and 85°N at perihelion (Bell et al., 2007; Bougher et al., 2006; Gonzalez-Galindo et al., 2009). GCM studies have revealed the importance of tides for TPW: Bell et al. (2007) showed upward propagating tides arising in the lower atmosphere shifted TPW toward the poles by 10° – 20° latitude but had little impact on the TPW amplitude, while Gonzalez-Galindo et al. (2009) showed tides generated in situ in the thermosphere were essential for TPW to occur and TPW effectively ceased without in situ tides. With regard to gravity waves, Medvedev and Yiğit (2012)'s Martian general circulation simulations showed that gravity wave momentum flux deposition (i.e., “drag”) modulated the latitudinal warming trend by shifting the minimum temperature from the equator to mid-latitudes, and effectively increasing the warming rate with latitude. Medvedev et al. (2013) simulations demonstrated that the dynamical and thermal effects of GWs together contribute to the enhancement of the middle atmosphere warming as well as of TPW.

Observations of aphelion TPW have suggested a weak warming trend, but have generally been inconclusive. As mentioned earlier, Bougher et al. (2006) found no conclusive evidence of TPW in their mostly dayside observations. However, Bougher et al. (2006) also analyzed a smaller subset of data from the nightside, the majority of which were measured at latitudes higher than where aphelion TPW is expected based on simulations by Bell et al. (2007). Lillis et al. (2008) used MGS electron reflectometry measurements to probe atmospheric density at 180 km and local time of 2.0 hr, and found slight density enhancements that could possibly be attributed to TPW for some MYs but not others. Forget et al. (2009), using nightside stellar occultation measurements during MY 28 from the Spectroscopy for Investigation of Characteristics of the Atmosphere of Mars (SPICAM) instrument onboard the Mars Express orbiter, found a $\sim 20\text{K}$ warming trend in the mesosphere near 85 km, but this trend dissipated with altitude, becoming undetectable near 105 km.

2. Data and Methods

This study uses exobase temperatures derived from solar occultation measurements made by the Extreme Ultraviolet Monitor (EUVM; Eparvier et al., 2015) onboard the Mars Atmosphere and Volatile EvolutionN (MAVEN; Jakosky et al., 2015) orbiter. Solar occultations inherently measure exactly at sunrise (hereafter, dawn) and sunset (hereafter, dusk). CO_2 densities and temperatures from ~ 100 to 200 km are derived from measurements by the EUVM 17–22 nm channel using the method of Thiemann et al. (2018). The observations are inherently constrained to local times at the solar terminator (i.e., either at dawn or dusk). Exobase temperature is found by first fitting the measured temperature profile to the Bates (1959) thermospheric temperature equation,

$$T(z) = T_{\text{exo}}\{1 - a \cdot e^{-\tau\varphi}\} \quad (1)$$

which was originally derived for Earth but applicable to Mars due to similarities in the planets' thermospheric structure (Bougher & Roble, 1991). Here, T is temperature, z is altitude, T_{exo} is exospheric temperature, φ , is the geopotential height,

$$a = 1 - \frac{T(z_0)}{T_{\text{exo}}} \quad (2)$$

and

$$\tau = \frac{1}{T_{\text{exo}} - T(z_0)} \left(\frac{dT}{dz} \right)_{z=z_0}, \quad (3)$$

where z_0 is some reference altitude above the mesopause. The Levenberg-Marquardt approach (e.g., Press, 2007) is used to fit these three parameters to the EUVM-measured temperature profiles. This study takes the exobase temperature to be the Bates temperature fit value at 180 km, the approximate altitude of the exobase.

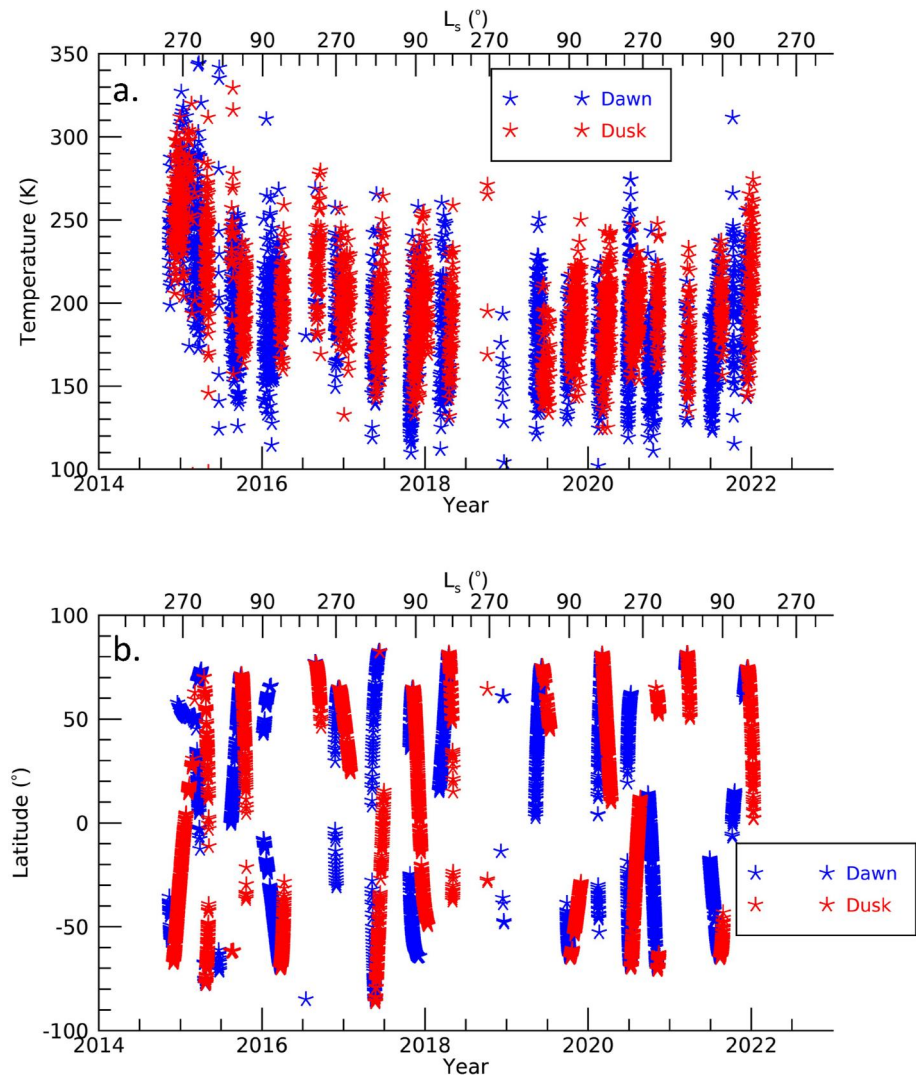


Figure 1. Time series of exobase temperatures (a) and corresponding observation latitudes (b). Red (blue) asterisk corresponds with dusk (dawn) observation local time. Mars Years increment at $L_s = 0$ with Mars Year 33 beginning in 2015.

The exobase temperature uncertainty is $\sim 12\%$ and found from a Monte-Carlo analysis using 100 randomized synthetic observations of atmospheres from the Mars Global Ionosphere Thermosphere Model (M-GITM; Bougher et al., 2015), where latitude, longitude and local-time were randomly selected. Component-level uncertain parameters in the instrument measurement equation are randomized in the same manner as done in Thiemann et al. (2018) for estimating the EUVM SO density measurement uncertainties. The combined solar occultation measurement and temperature retrieval uncertainty is found by comparing the retrieved, Bates-fitted temperatures at 180 km to those from the “ground truth” M-GITM atmospheres.

The exobase temperature for the entire period analyzed is shown in Figure 1a versus time (bottom axis) and L_s (top axis). Observations measured at dawn (3,075 observations) and dusk (2,922 observations) are shown with blue and red asterisks, respectively. The decreasing temperature trend from 2015 through 2018 is primarily due to the declining solar activity. The increasing temperature values in 2021 are primarily due to the increasing solar cycle. The local maxima (minima) near $L_s = 251^\circ$ ($L_s = 71^\circ$) are from the Mars orbit eccentricity, with perihelion (aphelion) occurring at that time. Figure 1b shows the corresponding observation latitudes, which vary as the spacecraft orbit precesses. The maximum latitude is seasonally dependent via the terminator location.

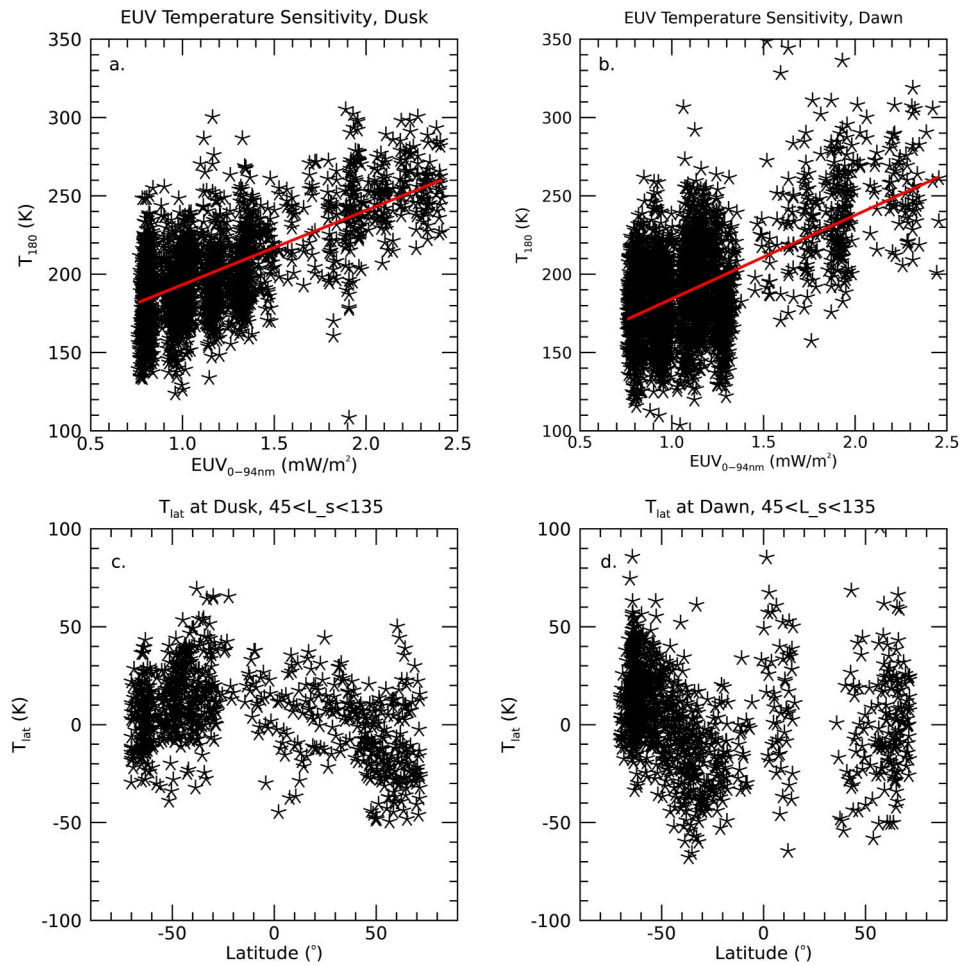


Figure 2. Exobase temperature variations versus EUV irradiance and latitude. (a, b) Exobase temperature versus EUV irradiance at dusk and dawn, respectively. (c, d) Exobase temperature with EUV variability removed versus latitude for $45^\circ < L_s < 135^\circ$ at dusk and dawn, respectively (north is positive).

The dominant solar EUV-induced temperature effects are removed from the data to better characterize TPW as follows: EUV irradiances are first calculated from the MAVEN/EUVM Level 3 spectral irradiance data (Thiemann et al., 2017) by integrating values from 0 to 93 nm, wavelengths capable of ionizing CO_2 . EUV irradiance effects are then detrended from the T_{exo} data by first finding a linear fit between T_{exo} and the ionizing EUV irradiance and subtracting the fit from the data. This process is illustrated in Figure 2, where panels a and b show the linear fits of T_{exo} versus EUV irradiance at dusk and dawn, respectively. EUV irradiance effects are detrended from the data by subtracting the fit from the data. Figures 2c and 2d show the resulting EUV-detrended temperatures for 90° of L_s centered at aphelion, $45^\circ < L_s < 135^\circ$.

3. Results

TPW at aphelion is evident at dawn in Figure 2d from the marked increase in temperature with southward latitude at dawn in the southern (winter) hemisphere. The corresponding dusk temperatures in Figure 2c show a temperature maximum near 35°S , with decreasing temperature toward the poles. In the dusk northern hemisphere, the predominant feature is overall a decreasing temperature trend with increasing latitude, indicative of adiabatic cooling in the summer hemisphere by the dayside ascending leg of the meridional circulation cell that causes TPW in the winter hemisphere (Gonzalez-Galindo et al. (2009)). We speculate this trend is not evident at dawn because dawn temperatures are less sensitive to dynamical processes occurring at later hours on the dayside.

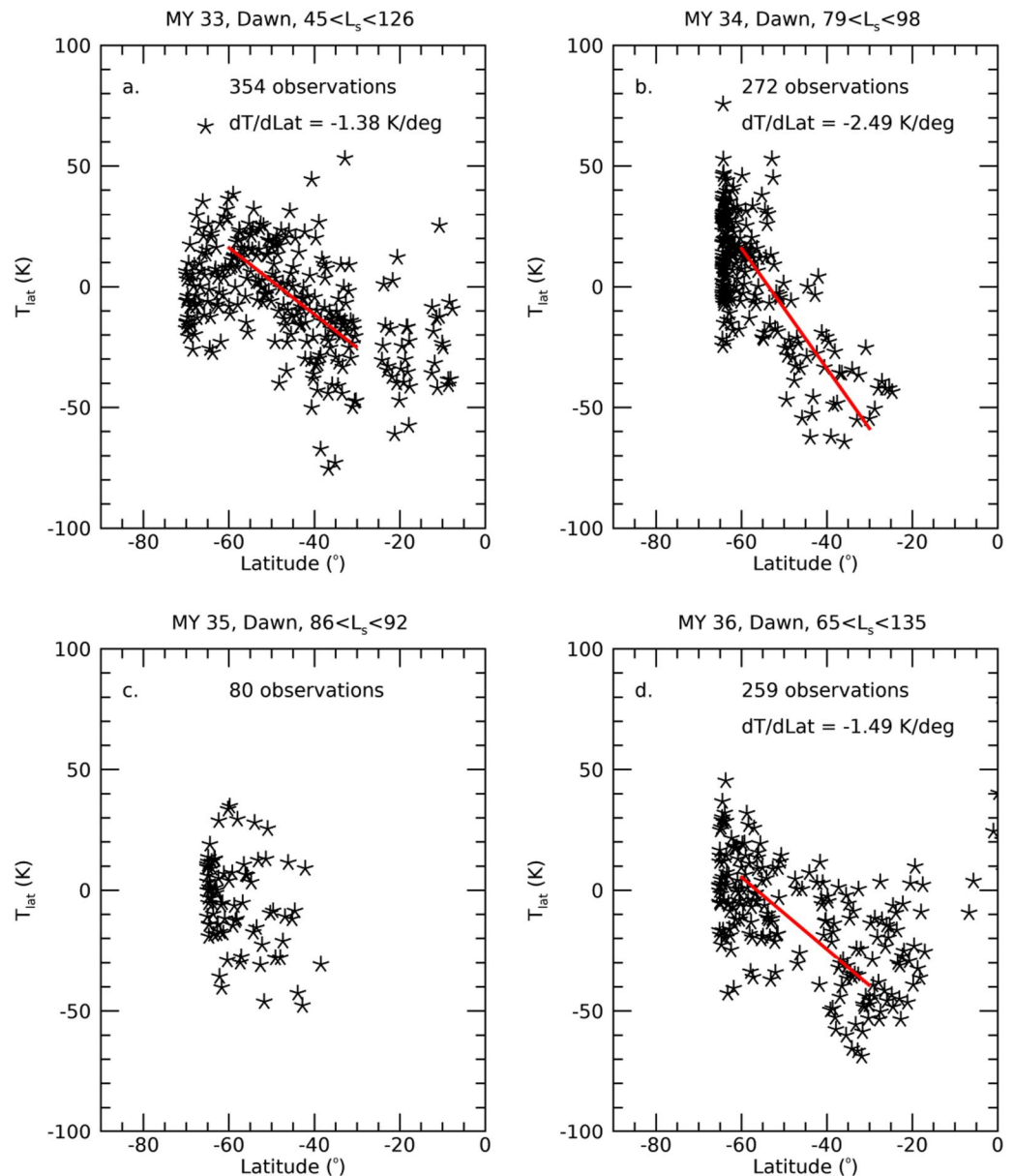


Figure 3. Detrended exobase temperatures versus latitude for individual MYs with the corresponding MY shown above each panel along with the L_s values spanned by the data. Linear fits of temperature versus latitude are overplotted in red; see text for details. No fit was found for MY 35 in (c).

Figure 3 shows the EUV-detrended exobase temperatures at aphelion for the southern hemisphere separated according to MY. For each MY, data are filtered for $45^\circ < L_s < 135^\circ$. The actual L_s range spanned by the available data for each MY is listed above each panel. The corresponding number of observations are printed on each panel. Each MY shown except MY 35 shows a clear TPW warming trend with increasing southward latitude. The sampling for MY 35 is significantly sparser than the other three years and, in particular, lacks data equatorward of -35° . For this reason, it cannot be concluded that no TPW occurred during MY 35. For the three MY showing a clear temperature trend with latitude, linear fits of the data between -60° and -30° are overplotted and the slopes of these fits are reported on the corresponding figure panels. The warming trend slopes for MY 33 and MY 36 are approximately the same, while the warming trend slope for MY 34 is $\sim 70\%$ higher than the other two years. However, it is important to note that the MY 34 data span a significantly narrower range of L_s centered near $L_s = 90^\circ$ than MY 33 and MY 36, and differences in the warming trend may be due to differences in the L_s range sampled.

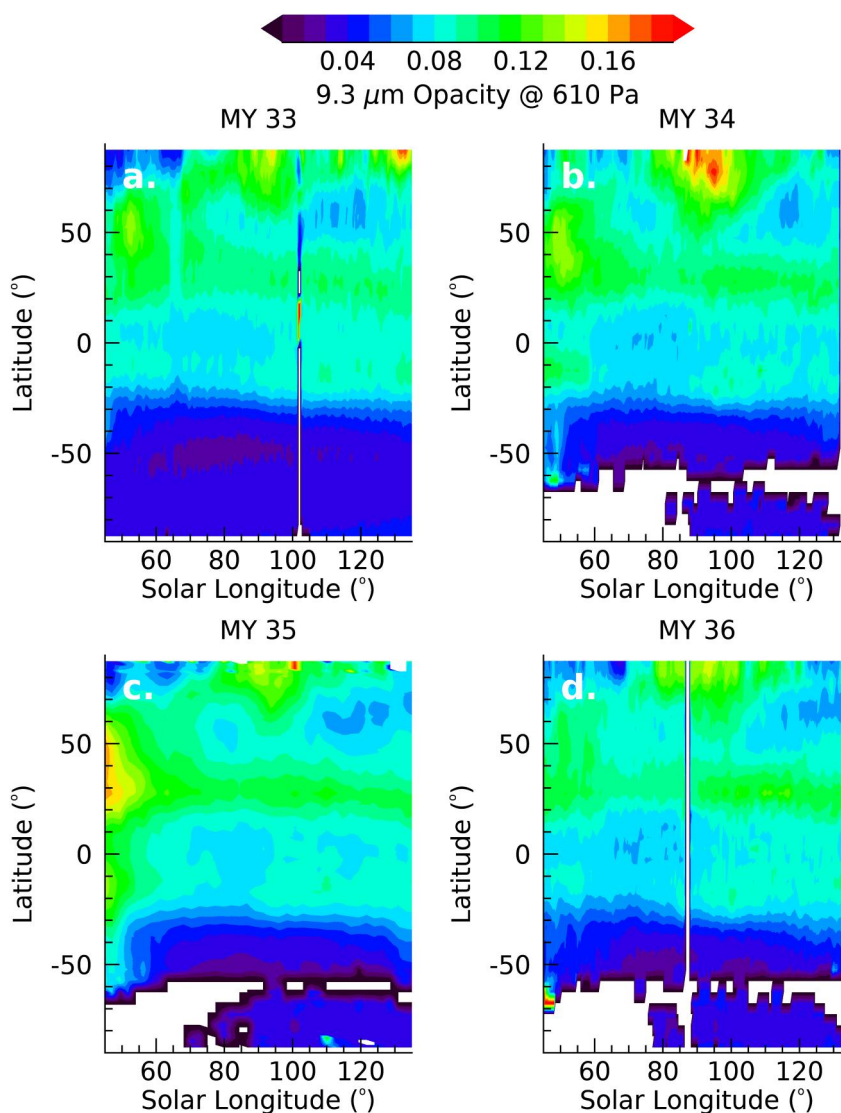


Figure 4. Distribution of atmospheric dust versus latitude and solar longitude. Panels show the $9.3\ \mu\text{m}$ absorption column dust optical depth normalized to the 610 Pa pressure level from Montabone et al. (2015, 2020) for the four MYs shown in Figure 3.

Since TPW is expected to depend on dust activity in the opposite hemisphere (Bell et al., 2007), dust distribution maps showing the $9.3\ \mu\text{m}$ absorption column dust optical depth versus latitude and solar longitude normalized to the 610 Pa pressure level from Montabone et al. (2015, 2020) are shown in Figure 4. The dust distributions are similar for all four MY with the notable difference being a marked increase in dust from a regional dust storm near the north pole around aphelion for MY 34. Given that MY 34 is also the year with the steepest TPW trend, it is likely this dust storm contributed to the increased TPW for this year based on the theoretical work by Bell et al. (2007).

The Nadir and Occultation for Mars Discovery (NOMAD) instrument (Vandaele et al., 2018) onboard the Trace Gas Orbiter (TGO) started solar occultation observations in MY 34 Ls 163° . The NOMAD temperature values have been retrieved with the same method as described in Trompet et al. (2023) using CO_2 lines in the spectral range of $3,708\text{--}3,738\ \text{cm}^{-1}$, and are used to corroborate the MAVEN/EUVM observations. The data set presented here contains 1,858 retrieved profiles over the 3,542 occultations made by NOMAD-SO from MY 34 Ls 163 to the end of MY 36. Solar EUV irradiance variability is removed from the NOMAD temperatures measured at 150 km using the same process applied to the EUVM data described in Section 2. The combined MY 35–36

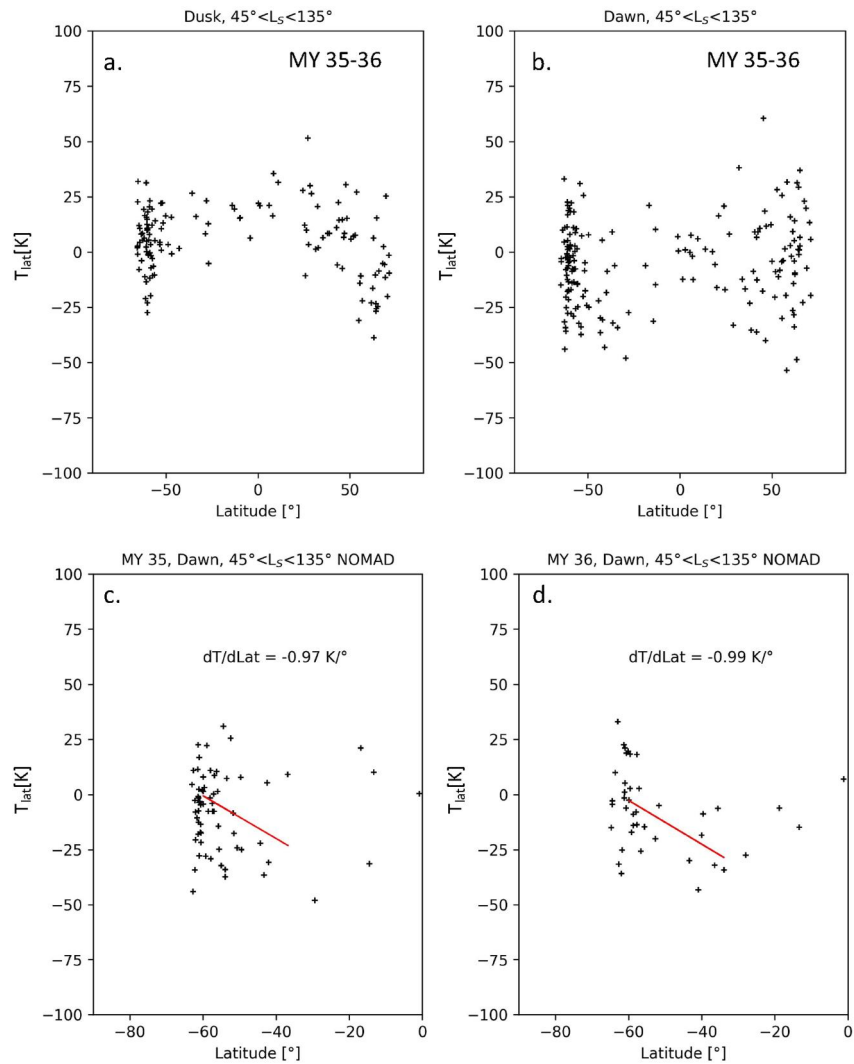


Figure 5. Temperature measurements at 150 km by TGO/NOMAD near aphelion. (a, b) EUV irradiance detrended temperatures for MY 35–36 at dawn and dusk, respectively. Individual MY temperatures at dawn shown for (c) MY 35 and (d) MY 36.

aphelion data are shown in Panels a and b of Figure 5 for dusk and dawn, respectively. These data are consistent with the EUVM observations, showing a warming trend near the poles at dawn and a cooling trend at dusk. Panels c and d of Figure 5 show aphelion temperatures measured at dawn for MY 35 and 36, respectively. For both MY 35 and MY 36, some of the highest temperatures in the southern hemisphere occur near the poles, but the warming trend with southward latitude is more distinct in MY 36, consistent with the MAVEN/EUVM observations.

Simulation results from the Mars Climate Database v6.1 (Forget et al., 1999; Madeleine et al., 2011; Millour et al., 2014) provide insight into the solar occultation observations. Figure 6a uses solid and dashed curves to show MCD predicted temperature differences relative to the southern hemisphere approximate maximum value (located at 50°S) at 150 km versus latitude at the EUVM SO observing local-times (dawn and dusk) for MY 33 and 34 at $L_s = 90$. The EUV-detrended EUVM SO measurements at 150 km (with a 5-sample boxcar smooth applied) are overplotted relative to their southern hemisphere approximate maximum value (located at 60°S) using dot-dashed curves. Figure 6b shows the global temperature structure at 150 km for context with the dawn and dusk observation locations indicated by blue and red curves, respectively. At dawn, the simulations reproduce many of the features shown in the EUVM SO data including the steeper temperature gradients for MY 34 relative to MY 33 and the plateauing of temperatures at high latitudes. Additionally, in the northern hemisphere both the MCD simulations and EUVM SO data show MY 33 temperatures to be warmer than MY 34 temperatures.

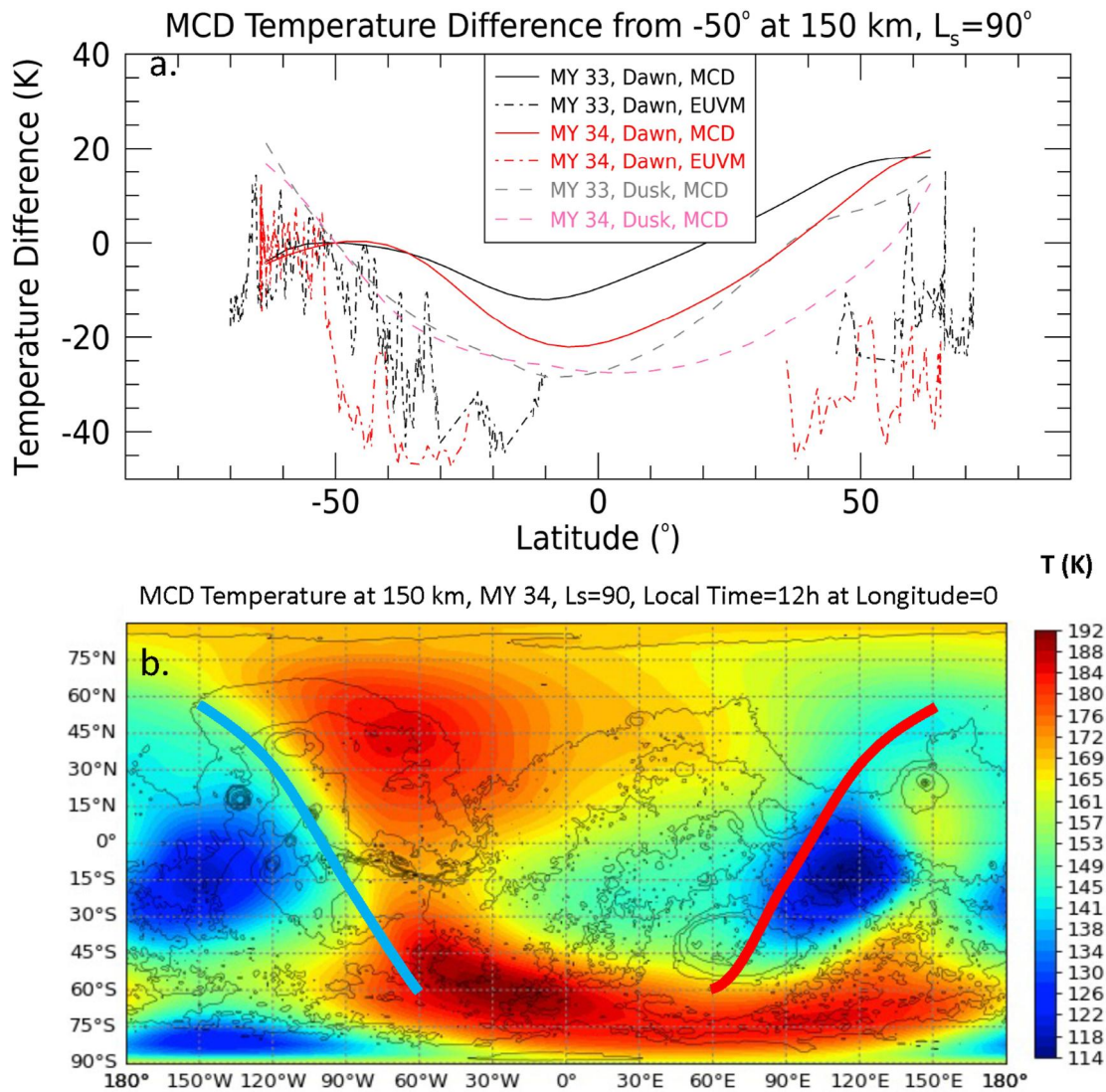


Figure 6. MCD simulation results: (a) Temperature difference relative to -50° Latitude at 150 km for the solar occultation observation locations at dawn and dusk for MY 33 and 34, $L_s = 90$. Dawn EUVM SO temperature difference data (5-sample smoothed) relative to -60° Latitude at 150 km are overplotted. (b) Global temperature at 150 km for MY 34. Overplotted blue and red curves correspond with dawn and dusk locations, respectively.

However, there are key differences between the simulations and measurements: (a) At dawn, the simulations show approximately 20 K less warming in the southern hemisphere from low to high latitudes than are found in the EUVM SO data; (b) the simulations show >40 K warmer temperatures in the northern hemisphere (relative to the southern hemisphere maximum) than found in the EUVM SO data; and (c) (at dawn) the simulations show the temperature plateauing approximately 15° northward of that found in the EUVM SO data. At dusk, the simulations do not reproduce the cooling trend toward the poles found in the EUVM SO data (shown Figure 2c) and instead show a warming trend toward the poles.

4. Discussion and Conclusions

Figures 2c and 2d show that TPW at aphelion is local-time dependent, with a more significant warming in the winter hemisphere at dawn and a more significant cooling in the summer hemisphere at dusk. This local-time sensitivity explains why Bougher et al. (2006) did not see evidence of TPW with the available aphelion data, which was predominantly measured near dusk, at a local time of 15.0 hr. This local-time dependence is not reproduced by the MCD global temperature maps, which show steeper TPW at dusk than dawn.

Dust in the summer hemisphere appears to be an important driver of TPW at aphelion, as predicted by Bell et al. (2007), given that the regional dust storm during MY 34 coincided with a ~70% steeper temperature gradient with latitude than that observed during MY 33 and 36. Dust-induced changes in the radiative properties of the atmosphere can significantly modulate the momentum balance and thus the mean flow and circulation. In addition, small-scale gravity waves substantially drive the variability and the general circulation of the atmosphere during dust storms (Yigit, 2023; Yigit et al., 2021).

Comparison with simulations suggested that the MCD reproduces some of the observed features but not others. Notably, the MCD was able to reproduce increased TPW for MY 34 relative to MY 33 using MY 34 dust distributions. This supports the hypothesis that the rare aphelion northern hemisphere dust storm increased TPW in the opposite hemisphere, and the observed steeper temperature gradients are likely not an artifact due to sampling differences. The observations showing TPW peaking at higher latitudes than the MCD may indicate the tidal forcing in the MCD is too weak based on results from Bell et al. (2007) showing the sensitivity of TPW peak latitude on upward propagating tides. Additionally, the MCD was not able to reproduce the same degree of TPW as found in the EUVM SO data. This could be due to (a) the meridional circulation is not strong enough in the MCD at aphelion, (b) the in situ tides are too weak in the MCD, or (c) atmospheric wave effects, which drive the horizontal circulation and adiabatic heating/cooling, are not realistically captured in the model.

We have analyzed for the first time the local time variations of the thermospheric polar warming during aphelion using solar occultation (SO) measurements made by the Extreme Ultraviolet Monitor (EUVM) onboard the Mars Atmosphere and Volatile Evolution (MAVEN) spacecraft. The main inferences of our study are as follows:

1. The TGO/NOMAD measurements corroborate those by MAVEN/EUVM by also showing TPW at dawn.
2. MY 34 showed significantly more (~20 K) aphelion TPW than the other three MY analyzed. This increase is attributed to an uncommon northern hemisphere aphelion dust storm that strengthened the meridional circulation responsible for TPW.
3. The MCD generally reproduces the observed aphelion TPW at dawn. Notable model-measurement differences that may lead to further insight with additional study are the lack of the MCD to reproduce the (a) the same degree of TPW (observations show ~40 K more warming), (b) the plateauing of TPW at dawn near 60°S, and (c) the relatively high temperatures at the mid to high latitude northern hemisphere at both dawn and dusk.

Data Availability Statement

MAVEN EUVM data are publicly available at the NASA Planetary Data System available at Eparvier et al. (2023). TGO NOMAD data are located at the ESA Planetary Science Archive available at Vandaele et al. (2023). MCD v6.1 simulations outputs were retrieved using the Web Interface available at Millour et al. (2023). The multi-annual gridded dust map product used in this study is publicly available at Montabone et al. (2023).

Acknowledgments

EMBT would like to thank and acknowledge Laboratoire de Météorologie Dynamique for hosting the MCD and dust maps used in this study through a publicly accessible web interface. The NOMAD experiment is led by the Royal Belgian Institute for Space Aeronomy (BIRA-IASB), with Co-PI teams in the United Kingdom (Open University), Spain (IAA-CSIC) and Italy (INAF-IAPS). The treatment of NOMAD data received funding from the European Union's Horizon 2020 research and innovation programme under grant agreement No 1011004052. F.G.-G. was funded by Spanish Ministerio de Ciencia, Innovación y Universidades, the Agencia Estatal de Investigación and EC FEDER funds under project PID2022-137579NB-I00 and acknowledges financial support from the Severo Ochoa Grant CEX2021-001131-S funded by MCIN/AEI/10.13039/501100011033. This work was funded in part through the NASA Mars Data Analysis Program through Grant 80NSSC20K0941.

References

- Bates, D. R. (1959). Some problems concerning the terrestrial atmosphere above about the 100 km level. *Proceedings of the Royal Society of London - Series A: Mathematical and Physical Sciences*, 253, 451–462.
- Bell, J. M., Bougher, S. W., & Murphy, J. R. (2007). Vertical dust mixing and the interannual variations in the Mars thermosphere. *Journal of Geophysical Research*, 112(E12), E12002. <https://doi.org/10.1029/2006je002856>
- Bougher, S. W., Bell, J. M., Murphy, J. R., Lopez-Valverde, M. A., & Withers, P. G. (2006). Polar warming in the Mars thermosphere: Seasonal variations owing to changing insolation and dust distributions. *Geophysical Research Letters*, 33(2), L02203. <https://doi.org/10.1029/2005gl024059>
- Bougher, S. W., Pawlowski, D., Bell, J. M., Nelli, S., McDunn, T., Murphy, J. R., et al. (2015). Mars global ionosphere-thermosphere model: Solar cycle, seasonal, and diurnal variations of the Mars upper atmosphere. *Journal of Geophysical Research: Planets*, 120(2), 311–342. <https://doi.org/10.1002/2014je004715>
- Bougher, S. W., & Roble, R. G. (1991). Comparative terrestrial planet thermospheres: 1. Solar cycle variation of global mean temperatures. *Journal of Geophysical Research*, 96(A7), 11045–11055. <https://doi.org/10.1029/91ja01162>
- Eparvier, F. G., Chamberlin, P. C., Woods, T. N., & Thiemann, E. M. B. (2015). The solar extreme ultraviolet monitor for MAVEN. *Space Science Reviews*, 195(1–4), 293–301. <https://doi.org/10.1007/s11214-015-0195-2>
- Eparvier, F. G., Thiemann, E. M. B., Chamberlin, P. C., Templeman, B., & Borelli, R. (2023). The MAVEN EUVM level 2 data (version 14) [Dataset]. NASA PDS. Retrieved from <https://pds-ppi.igpp.ucla.edu/mission/MAVEN/MAVEN/EUV>
- Forget, F., Hourdin, F., Fournier, R., Hourdin, C., Talagrand, O., Collins, M., et al. (1999). Improved general circulation models of the Martian atmosphere from the surface to above 80 km. *Journal of Geophysical Research*, 104(E10), 24155–24175. <https://doi.org/10.1029/1999je001025>
- Forget, F., Montmessin, F., Bertaux, J. L., González-Galindo, F., Lebonnois, S., Quemerais, E., et al. (2009). Density and temperatures of the upper Martian atmosphere measured by stellar occultations with Mars Express SPICAM. *Journal of Geophysical Research: Planets*, 114(E1), E01004. <https://doi.org/10.1029/2008je003086>

- González-Galindo, F., Forget, F., López-Valverde, M. A., & Angelats i Coll, M. (2009). A ground-to-exosphere Martian general circulation model: 2. Atmosphere during solstice conditions—Thermospheric polar warming. *Journal of Geophysical Research*, *114*(E8), E08004. <https://doi.org/10.1029/2008je003277>
- Jakosky, B. M., Lin, R. P., Grebowsky, J. M., Luhmann, J. G., Mitchell, D. F., Beutelschies, G., et al. (2015). The Mars atmosphere and volatile evolution (MAVEN) mission. *Space Science Reviews*, *195*(1–4), 3–48. <https://doi.org/10.1007/s11214-015-0139-x>
- Lillis, R. J., Bougher, S. W., Mitchell, D. L., Brain, D. A., Lin, R. P., & Acuña, M. H. (2008). Continuous monitoring of nightside upper thermospheric mass densities in the Martian southern hemisphere over 4 Martian years using electron reflectometry. *Icarus*, *194*(2), 562–574. <https://doi.org/10.1016/j.icarus.2007.09.031>
- Madeleine, J.-B., Forget, F., Millour, E., Montabone, L., & Wolff, M. J. (2011). Revisiting the radiative impact of dust on Mars using the LMD global climate model. *Journal of Geophysical Research*, *116*, E11. <https://doi.org/10.1029/2011je003855>
- Medvedev, A. S., & Hartogh, P. (2007). Winter polar warmings and the meridional transport on Mars simulated with a general circulation model. *Icarus*, *186*(1), 97–110. <https://doi.org/10.1016/j.icarus.2006.08.020>
- Medvedev, A. S., & Yiğit, E. (2012). Thermal effects of internal gravity waves in the Martian upper atmosphere. *Geophysical Research Letters*, *39*(5), L05201. <https://doi.org/10.1029/2012gl050852>
- Medvedev, A. S., Yiğit, E., Kuroda, T., & Hartogh, P. (2013). General circulation modeling of the Martian upper atmosphere during global dust storms. *Journal of Geophysical Research: Planets*, *118*(10), 2234–2246. <https://doi.org/10.1002/2013JE004429>
- Millour, E., Forget, F., & Lewis, S. R. (2014). Mars climate database v. 5.1. User manual. *ESTEC Contract*, 11369, 95.
- Millour, E., Forget, F., & Lewis, S. R. (2023). Mars climate database web interface (version 6.1) [Dataset]. The Mars Climate Database Project. Retrieved from https://www-mars.lmd.jussieu.fr/mcd_python/
- Montabone, L., Forget, F., Millour, E., Wilson, R. J., Lewis, S. R., Cantor, B., et al. (2015). Eight-year climatology of dust optical depth on Mars. *Icarus*, *251*, 65–95. <https://doi.org/10.1016/j.icarus.2014.12.034>
- Montabone, L., Spiga, A., Kass, D. M., Kleinböhl, A., Forget, F., & Millour, E. (2020). Martian year 34 column dust climatology from Mars climate sounder observations: Reconstructed maps and model simulations. *Journal of Geophysical Research: Planets*, *125*(8), e2019JE006111. <https://doi.org/10.1029/2019je006111>
- Montabone, L., Spiga, A., Kass, D. M., Kleinböhl, A., Forget, F., & Millour, E. (2023). Martian gridded dust map. (Version 2.5) [Dataset]. The Mars Climate Database Project. Retrieved from http://www-mars.lmd.jussieu.fr/mars/dust_climatology/
- Press, W. H. (2007). Numerical recipes. In *The art of scientific computing* (3rd ed.). Cambridge University Press.
- Thiemann, E. M., Chamberlin, P. C., Eparvier, F. G., Templeman, B., Woods, T. N., Bougher, S. W., & Jakosky, B. M. (2017). The MAVEN EUVM model of solar spectral irradiance variability at Mars: Algorithms and results. *Journal of Geophysical Research: Space Physics*, *122*(3), 2748–2767. <https://doi.org/10.1002/2016ja023512>
- Thiemann, E. M. B., Eparvier, F. G., Bougher, S. W., Dominique, M., Andersson, L., Girazian, Z., et al. (2018). Mars thermospheric variability revealed by MAVEN EUVM solar occultations: Structure at aphelion and perihelion and response to EUV forcing. *Journal of Geophysical Research: Planets*, *123*(9), 2248–2269. <https://doi.org/10.1029/2018je005550>
- Trompet, L., Vandaele, A. C., Thomas, I., Aoki, S., Daerden, F., Erwin, J., et al. (2023). Carbon dioxide retrievals from NOMAD-SO on ESA's ExoMars trace gas orbiter and temperature profiles retrievals with the hydrostatic equilibrium equation: 1. Description of the method. *Journal of Geophysical Research: Planets*, *128*(3), e2022JE007277. <https://doi.org/10.1029/2022je007277>
- Vandaele, A. C., Lopez-Moreno, J. J., Patel, M. R., Bellucci, G., Daerden, F., Ristic, B., et al. (2023). The TGO NOMAD SO data (version 3) [Dataset]. PSA. Retrieved from <https://archives.esac.esa.int/psa/>
- Vandaele, A. C., Lopez-Moreno, J. J., Patel, M. R., Bellucci, G., Daerden, F., Ristic, B., et al. (2018). NOMAD, an integrated suite of three spectrometers for the ExoMars trace gas mission: Technical description, science objectives and expected performance. *Space Science Reviews*, *214*(5), 1–47. <https://doi.org/10.1007/s11214-018-0517-2>
- Yiğit, E. (2023). Coupling and interactions across the Martian whole atmosphere system. *Nature Geoscience*, *16*(2), 123–132. <https://doi.org/10.1038/s41561-022-01118-7>
- Yiğit, E., Medvedev, A. S., Benna, M., & Jakosky, B. M. (2021). Dust storm-enhanced gravity wave activity in the Martian thermosphere observed by MAVEN and implication for atmospheric escape. *Geophysical Research Letters*, *48*(5), e2020GL092095. <https://doi.org/10.1029/2020gl092095>